Cancer Research

Targeting EphA3 Inhibits Cancer Growth by Disrupting the Tumor Stromal Microenvironment

Mary E. Vail[1], Carmel Murone[2], April Tan[1], Linda Hii[1], Degu Abebe[1], Peter W. Janes[1], Fook-Thean Lee[2], Mark Baer[3], Varghese Palath[3], Christopher Bebbington[3], Geoffrey Yarranton[3], Carmen Llerena[1], Slavisa Garic[4], David Abramson[4], Glenn Cartwright[2], Andrew M. Scott[2,5], and Martin Lackmann[1,†]

Abstract

Eph receptor tyrosine kinases are critical for cell–cell communication during normal and oncogenic tissue patterning and tumor growth. Somatic mutation profiles of several cancer genomes suggest EphA3 as a tumor suppressor, but its oncogenic expression pattern and role in tumorigenesis remain largely undefined. Here, we report unexpected EphA3 overexpression within the microenvironment of a range of human cancers and mouse tumor xenografts where its activation inhibits tumor growth. EphA3 is found on mouse bone marrow–derived cells with mesenchymal and myeloid phenotypes, and activation of EphA3$^+$/CD90$^+$/Sca1$^+$ mesenchymal/stromal cells with an EphA3 agonist leads to cell contraction, cell–cell segregation, and apoptosis. Treatment of mice with an agonistic α-EphA3 antibody inhibits tumor growth by severely disrupting the integrity and function of newly formed tumor stroma and microvasculature. Our data define EphA3 as a novel target for selective ablation of the tumor microenvironment and demonstrate the potential of EphA3 agonists for anticancer therapy. *Cancer Res; 74(16); 4470–81. ©2014 AACR.*

Introduction

The intimate communication between cancer cells and host-derived stromal and myeloid cells (1), which are recruited from the bone marrow (2) and constitute the vascularized tumor microenvironment (TME), is critical for primary tumor growth, invasion, and metastasis (3). Among the proteins considered instrumental in establishing the TME (1), Ephs and their cell-associated ephrin ligands are implicated in neoangiogenesis and invasive tumor growth, and are increasingly being recognized as therapeutic targets entering clinical trials (4).

Ephs RTKs comprise A- and B-type receptors that interact preferentially with GPI-linked type-A ephrins, and transmembrane type-B ephrins, respectively. Their activation triggers context- dependent signaling pathways that control cell spreading, adhesion, cell migration, and (stem) cell proliferation. Ephs function also in the absence of kinase activity, usually with the opposite outcome, promoting cell-spreading, cell–cell adhesion, invasion, and supporting stem cell proliferation (5, 6).

Ephs and ephrins are commonly overexpressed in a broad range of cancers, where their oncogenic roles often reflect their dichotomous developmental activities. Thus, depending on tumor type and disease stage, overexpressed Ephs can promote or inhibit tumor progression (7–9). Importantly, oncogenic Eph expression often coincides with low or absent ephrin expression and kinase-independent functions (7, 10), whereas Eph activation by exogenous agonists typically inhibits proliferation, survival, and tumor growth (4, 5).

EphA3 is found in mesenchymal tissues of developing axial muscles, lung, kidney, and heart (11), is implicated in mesoderm (12), neural patterning (13), and is essential for endothelial-to-mesenchymal transition (EndMT) during heart development (14). There is very little evidence for physiologic adult expression or function, but EphA3 is overexpressed in solid and hematopoietic tumor cells (9, 15–17), and implicated in maintaining tumor-initiating cells in glioblastoma (9) and leukemia (18). Frequent somatic mutations of EphA3 in various metastatic cancers are thought to indicate a tumor suppressor role of the kinase-active receptor (19–22).

We now demonstrate, for the first time, conspicuous EphA3 expression predominantly in the stromal TME in a broad range of human solid tumors and mouse tumor xenografts. The

[1]Department of Biochemistry and Molecular Biology, Monash University, Victoria, Australia. [2]Ludwig Institute for Cancer Research, Melbourne, Victoria, Australia. [3]KaloBios Pharmaceuticals, Inc., South San Francisco, California. [4]Faculty of Information Technology, Monash University, Clayton, Victoria, Australia. [5]Faculty of Medicine, University of Melbourne, Victoria, Australia.

Note: Supplementary data for this article are available at Cancer Research Online (http://cancerres.aacrjournals.org/).

†Deceased.

A.M. Scott and M. Lackmann share senior authorship of this article.

Corresponding Authors: Mary E. Vail, Department of Biochemistry & Molecular Biology, Monash University, Clayton Campus, Clayton, Victoria 3800, Australia. Phone: 613-9902-9338; Fax: 613-9902-9500; E-mail: mary.vail@monash.edu; Andrew M. Scott, Ludwig Institute for Cancer Research, Level 5, Olivia Newton-John Cancer & Wellness Centre, Austin Health, 145-163 Studley Road, Heidelberg, Melbourne, Victoria 3084, Australia; E-mail: Andrew.Scott@ludwig.edu.au; and Martin Lackmann, Department of Biochemistry & Molecular Biology, Monash University, Clayton, Victoria 3800, Australia; E-mail: Martin.Lackmann@monash.edu.

doi: 10.1158/0008-5472.CAN-14-0218

EphA3-activating mAb IIIA4 (23) targets bone marrow–derived mesenchymal/stromal and myeloid EphA3$^+$ cells in the tumor microenvironment, and EphA3$^+$/CD29$^+$/CD90$^+$/Sca1^{high} mesenchymal–stromal/stem cells (MSC) respond to IIIA4 with EphA3 phosphorylation, rapid cell contraction, and apoptosis. In xenograft models, IIIA4 treatment significantly inhibits tumor growth by disrupting the overall stromal and vascular tissue architecture and function.

The prominent expression and function of EphA3 in the TME but not in normal tissues, together with favorable clinical properties of the humaneered IIIA4 mAb (KB004) reported from phase I trials (24), indicate exciting potential therapeutic opportunities for solid tumor treatment.

Materials and Methods

Antibodies and reagents

A list of antibodies and reagents is provided in the Supplementary Data.

Cell lines and culture

Human DU145 (ATCC HTB-81), 22RV1 (ATCC CRL-2505), and LnCaP (ATCC CRL-1740), and mouse LLC (ATCC CRL-1642) are authenticated, karyotyped cell lines from ATCC. EphA3/293 cells were derived (23) from HEK293T cells (ATCC CRL-3216) and maintained in DMEM 10% FCS/G418/zeocin, 5% CO_2. LIM2550 cells (25), generated at the Ludwig Institute (Melbourne, Australia), and all ATCC cell lines were maintained in RPMI/10% FCS/10% CO_2. Cell lines were kept in continuous culture for <10 passages and tested (PCR, FACS) before experimental use for phenotype and expression of relevant proteins.

Mouse xenografts, antibody treatment, and GFP bone marrow reconstitution

Animal procedures were according to Monash University and Austin Hospital Animal Ethics Committee guidelines. BALB/c$^{nu/nu}$ mice (4–6 weeks, ARC), subcutaneously injected with 1×10^7 DU145, 22Rv1, or LIM2550 cells, were treated by intraperitoneal injection (2/week) of antibodies or PBS when tumors reached approximately 100 mm^3. For bone marrow transplantation, BALB/c$^{nu/nu}$ mice (4 weeks old), within 48 hours of irradiation (2 × 5.25 Gy), were intravenously injected with 1×10^7 freshly isolated bone marrow cells from BALB/c$^{nu/nu}$ or GFP transgenic mice [Tg(CAG-EGFP)1Osb/J, Jackson Laboratory], 4 to 6 weeks before tumor xenografting. Bone marrow cells were depleted by MACS (Miltenyi Biotec) or FACS from EphA3$^+$ cells using Alexa^{647}chIIIA4; control bone marrow was prepared by applying unlabeled cells to the MACS.

Hypoxia measurement

Mice were injected, 30 minutes before analysis, with 60 μg/g pimidazole (Hypoxyprobe HPI, Inc.), optimum cutting temperature (OCT)-frozen tumor sections analyzed with [FITC]-α-pimidizole/[HRP]α-FITC antibodies. Olympus CellSens software was used for quantitation ($n \geq 3$ mice/group, 10 fields of view).

In vivo multiphoton and live cell microscopy

For intravital multiphoton imaging (Leica SP5, 20× Plan Apo-1.0-NA water lens, 4 external detectors), subcutaneous tumors were exposed by generating skin flaps through incisions along the ventral midline. Qdot^{655}chIIIA4 (0.025 mg) was tail vein injected 48 hours before imaging, and 0.1 mL Ricinus Communis Agglutinin (RCA)-lectin[FITC]; 5 mg/mL] was added immediately before imaging to label blood vessels (26). Intrinsic Second Harmonic Generation (SHG) signals were used to reveal collagen fibers (27). To monitor vasculature integrity, mice were injected 30 minutes before imaging with 0.1 mL [FITC]lectin and 15 μL Qtracker 655.

Leica SP5 inverted confocal microscopes (63× glycerol objective, NA 1.3) were used for imaging live cells or 4% PFA-fixed cells.

3D image analysis

Imaris 7.3.1 Software (Bitplane) was used for three-dimensional (3D) reconstruction and image analysis of 2-photon microscope Z-stacks (1–5 μm sections). Total fluorescent isosurfaces and ratios between fluorescent channels were determined by thresholding of individual channels, volume rendering of Z-stacks, and applying isosurfaces to thresholded regions (constant threshold values for all samples in one experiment). A minimum of 3 to 10 regions, 3 mice per experiment were analyzed.

Tissue immunohistochemistry and immunofluorescence microscopy

OCT-embedded fresh-frozen human tissue samples from surgical biopsies between 1995 and 2007 (Austin Health Tissue Bank), or from resected tumor xenografts, sectioned (6 μm) and fixed (10 minutes, acetone) were stained (Vector Labs ABC Kit), Hematoxylin counterstained and imaged (Olympus DotSlide). GFP$^+$ tumor tissues were fixed in 4% PFA overnight at 4°C and transferred to 30% sucrose overnight before freezing in OCT and sectioning. For immunofluorescence microscopy (IFM), directly conjugated primary or secondary antibodies were used, nuclei counterstained with Hoechst, and imaged on Leica AF6000 or SP5 microscopes.

2D image analysis

Microscopic images (Leica AF6000, 40× objective) of tumor sections (≥10 fields of view/tumor, ≥3 mice/group) and fluorescent live cell images were quantitated (ImageJ) using thresholded fluorescent channels. ImageJ macros were adopted into a Kepler workflow software (28) for unbiased quantification to threshold and calculate total fluorescent area per field (for tenascin and nuclei) or binarized for particle detection to count individual vessels per field.

Tumor MSC isolation

Single-cell suspensions, filtered (40- and 20-μm sieves) from Collagenase Type 3/Deoxyribonuclease I (Worthington)-digested tumors and treated with Red Blood Cell Lysis Buffer (Sigma-Aldrich), were FACSed (Influx, BD Biosciences) for EphA3/CD90/Sca-1 expression and sorted cells maintained (10,000 cells/well, 6-well plate) at 2% O_2/5% CO_2/37°C in

DMEM/10% FBS/penicillin/streptomycin, leukemia inhibitory factor (1,000 U/mL; Millipore), EGF (10 ng/mL; Invitrogen), PDGF (10 ng/mL; Invitrogen). Osteogenic, adipogenic, and chondrogenic MSC differentiation media were from Invitrogen.

Viability assay

Tumor MSCs were treated as indicated in figures and viability assessed by propidium Iodide exclusion. Apoptosis of adherent cells was imaged using a TUNEL kit (In Situ Cell Death Detection Kit, Roche). MSCs on fibronectin-coated polystyrene slides were treated as described in the figure. Fractions of apoptotic nuclei were determined from "thresholded", binarized fluorescence channels using particle counting (ImageJ, version 1.46r).

Immunoprecipitation and Western blotting

IIIA4 α-EphA3 mAb (23) immunoprecipitates from (0.15 mg total protein) tumor cell lysates or frozen tumor homogenates were Western blotted with indicated antibodies, and actin blots of total protein lysate (10 μg) were used as a loading control. Blots were visualized using ECL (Supersignal, Thermo Fisher Scientific).

Flow cytometry

A LSRII flow cytometer (Becton Dickinson) was used for flow cytometry, dead cells detected with propidium iodide, and FLOWJO software (TreeStar) used for raw data analysis and multivariate compensation.

Statistical analysis

GraphPad and Microsoft Excel (Microsoft) were used to estimate mean ± SE, unpaired two-tailed *t* tests (two variables) and two-way ANOVA (multiple parameters). For tumor treatments, one-way ANOVA with a Bonferroni *t* test as pairwise *post hoc* analysis was used.

Results

Preferential expression of EphA3 in tumor stroma and vasculature

Compared with other Ephs, the expression profile of EphA3 in tumors has remained poorly characterized. Using the IIIA4 mAb, previously used for the isolation and functional characterization of EphA3 (29–31), our immunohistochemical expression analysis revealed EphA3-specific staining in 95% (154 of 162) of human tumor tissues from a broad range of cancer types (Supplementary Table S1). α-EphA3 and α-CD31 immunohistochemistry (IHC) of successive tumor tissue sections, and IFM with combinations of IIIA4 and α-CD31 or α-Vimentin antibodies (Fig. 1A and Supplementary Fig. S1A), showed that in most cases EphA3 is present in the vascularized (89%) or stromal (71%) TME (Supplementary Table S1), but less frequent in tumor cells. Organ-matched nontumor samples from all patients showed little detectable IIIA4 staining (Fig. 1A, insets; Supplementary Fig. S1A). Indeed, immunoprecipitation (IP) analysis of human tumor cell lines indicated the lack of EphA3 in all tested colon and lung carcinoma cells, while in agreement with previous studies (16), several primary melanoma cell lines were EphA3$^+$ (Supplementary Fig. S1D). Also, analysis of experimental tumors from EphA3$^-$ mouse lung carcinoma (LLC) and human prostate (DU145) and colon carcinoma cells (LIM2250) indicated EphA3 in tumor lysates, but not in the corresponding cell lines (Fig. 1B and C). IHC confirmed α-EphA3 immunoreactivity in areas of the tumor xenografts that stained with antibodies against stromal and vascular markers, particularly within the rim of EphA3$^-$ (DU145, LIM2550) and EphA3$^+$ 22RV1 tumor xenografts (Fig. 1D). In contrast, nonstromal DU145 tumor tissue, all of the tested normal adult mouse tissues, and established mouse endothelial cell lines (not shown) lacked EphA3 expression (Supplementary Figs. S1C and S2A–S2C).

The chIIIA4 α-EphA3 mAb selectively targets tumor stroma and vasculature

We studied therapeutic targeting of the EphA3$^+$ tumor stroma by comparing EphA3$^+$ 22RV1 and EphA3$^-$ DU145 prostate carcinoma xenografts, the latter displaying EphA3 stromal and vascular staining reminiscent of that observed in human prostate carcinomas (Fig. 1A and D and Supplementary Fig. S1C). For ease of EphA3 detection in these and other experiments, we used a recombinant chimeric (ch) version of the IIIA4 mAb (23), where the mouse IIIA4 variable IgG region is fused to human Igγ-1 and Igκ constant regions, retaining the affinity (Supplementary Table S2), specificity, and tumor-targeting capacity (Supplementary Fig. S3A–S3C) of mouse IIIA4. IFM of tumors from chIIIA4-injected mice confirmed its dose-dependent accumulation, significantly stronger in EphA3$^+$ 22RV1 xenografts than in EphA3$^-$ DU145 xenografts (Supplementary Fig. S4A–S4C).

We assessed chIIIA4 tumor targeting *in vivo*, by imaging subcutaneous Du145 xenografts in mice injected with ^{655}Qdot-tagged chIIIA4, and with FITC-tagged RCA lectin ([FITC] lectin) marking blood-perfused vessels (5, 32). Intravital Multiphoton microscopy revealed ^{655}Qdot-chIIIA4 within stromal tissue and around blood vessels within the tumor (Fig. 2A, tumor), but not within the adjacent normal mouse skin (Fig. 2A, skin). Confocal microscopy confirmed binding of the injected chIIIA4 (Fig. 2B), but not of an isotype-matched control mAb (Fig. 2C), to some CD31$^+$ tumor vessels, whereas flow cytometry of cell suspensions revealed that 13.6% of the EphA3$^+$ cells in these tumors (14.2% of total) were also [FITC]lectin$^+$ (Fig. 2D). Furthermore, confocal microscopy indicated that also in 22RV1 xenografts, Tenascin-C$^+$ stromal cells and some [FITC]lectin-labeled tumor vessels are targeted by chIIIA4 (Fig. 2E).

EphA3 is expressed on bone marrow–derived MSCs that promote tumor growth

We next studied the phenotype and tissue origin of EphA3$^+$ stromal cells. FACS analysis of single-cell suspensions from day 21 (~0.2 cm^3) DU145 or LIM2550 (not shown) tumors yielded a population of EphA3$^+$ cells expressing myeloid, MSC, and endothelial surface markers (Supplementary Fig. S5A). To isolate tumor stroma–derived cells capable of *ex vivo* expansion, sorting for EphA3$^+$/CD90$^+$/Sca-1^{Hi} cells consistently yielded a small population of adherent cells (Supplementary Fig. S5B and C), the only population that allowed propagation

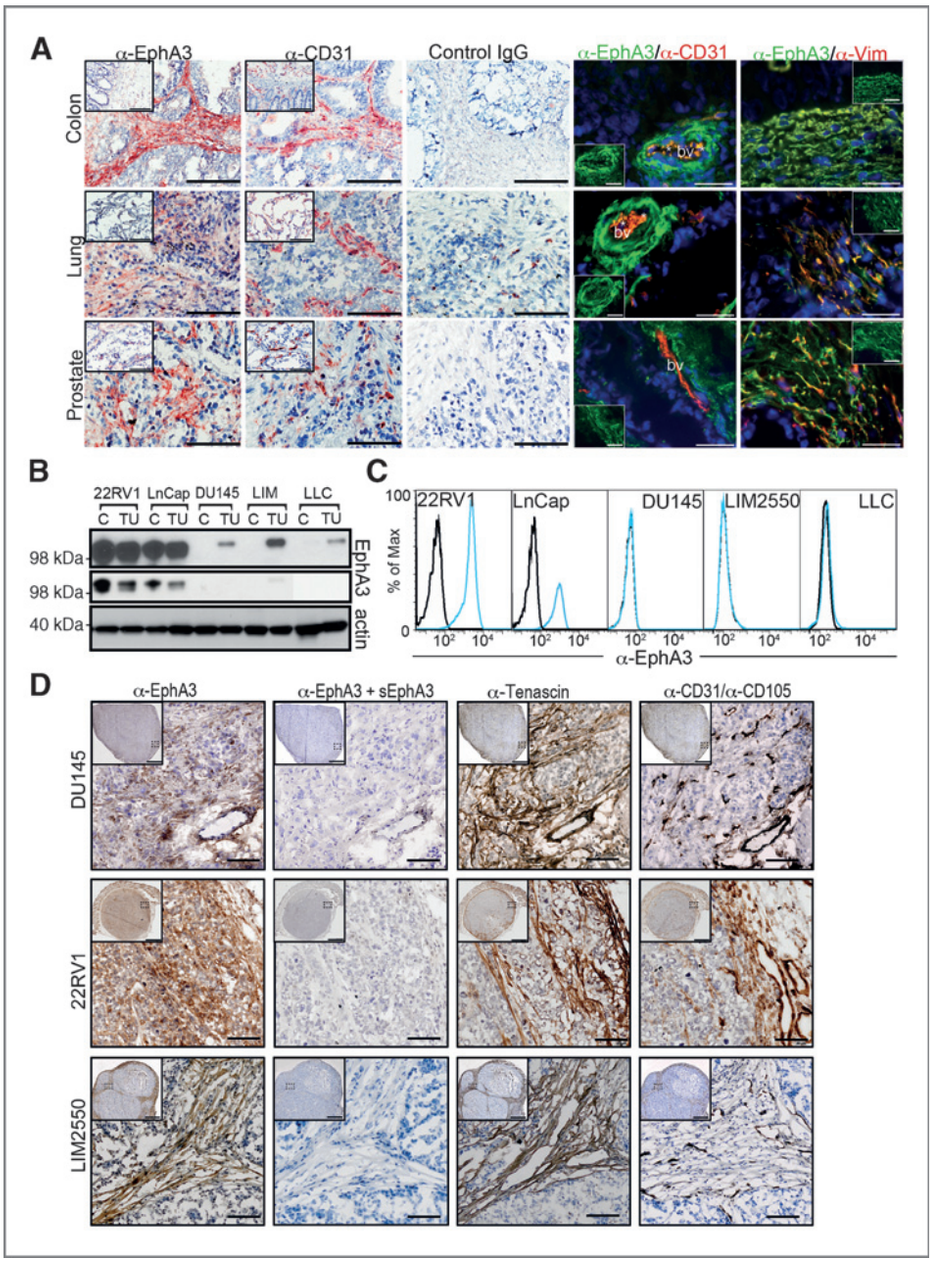

Figure 1. EphA3 is expressed in stromal and vascular tissues of human tumors and mouse xenografts. A, representative IHC of human colon, lung, and prostate tumor sections probed with α-EphA3 (IIIA4), α-CD31, and a nonrelevant control antibody. Insets, matched nontumor samples; scale bars, 0.1 mm. Two rightmost columns show IFM of EphA3/CD31 and EphA3/vimentin coexpression, using secondary Alexa^{488} (α-EphA3) and Alexa^{555} (α-CD31, α-Vimentin) conjugated antibodies; insets show individual α-EphA3 fluorescence micrographs. Scale bars, 50 μm. B, IP/Western blot analysis of EphA3^{+}-prostate (22RV1, LnCap), and EphA3^{-}-prostate (DU145), colon (LIM2550), and lung (Lewis Lung Carcinoma, LLC) tumor cell lines (C) and derived solid tumor xenografts (TU). Middle and top, dark and light exposure of the same blot to reveal intensity differences masked in overexposed lanes. C, flow cytometry of indicated tumor cell lines, EphA3^{+} cells in blue. D, IHC of corresponding tumor xenografts to detect microvasculature (α-CD31, α-CD105), stroma (with α-Vimentin), and EphA3 (IIIA4 mAb). Control sections were developed with α-EphA3 in the presence of 20-fold excess soluble human EphA3 (sEphA3); scale bars, 50 μm. Insets show whole tumor, and magnified areas are indicated by boxes; scale bars, 1 mm.

at clonal seeding density (10 cells/well, 18%–30% of wells). The expanded adherent cells expressed typical MSC cell surface markers (33, 34), including Sca-1, CD29, CD90, CD105, CD106, CD146, and CD44^{low}, but lacked typical myeloid and endothelial markers (Supplementary Fig. S5D). Importantly, the cell surface marker expression profile of these tumor-derived MSCs was almost identical to that of bone marrow–derived MSCs (33) isolated from crushed femurs of the same DU145 tumor-bearing mice (Fig. 3A), and both MSC populations differentiated in corresponding culture media into osteogenic,

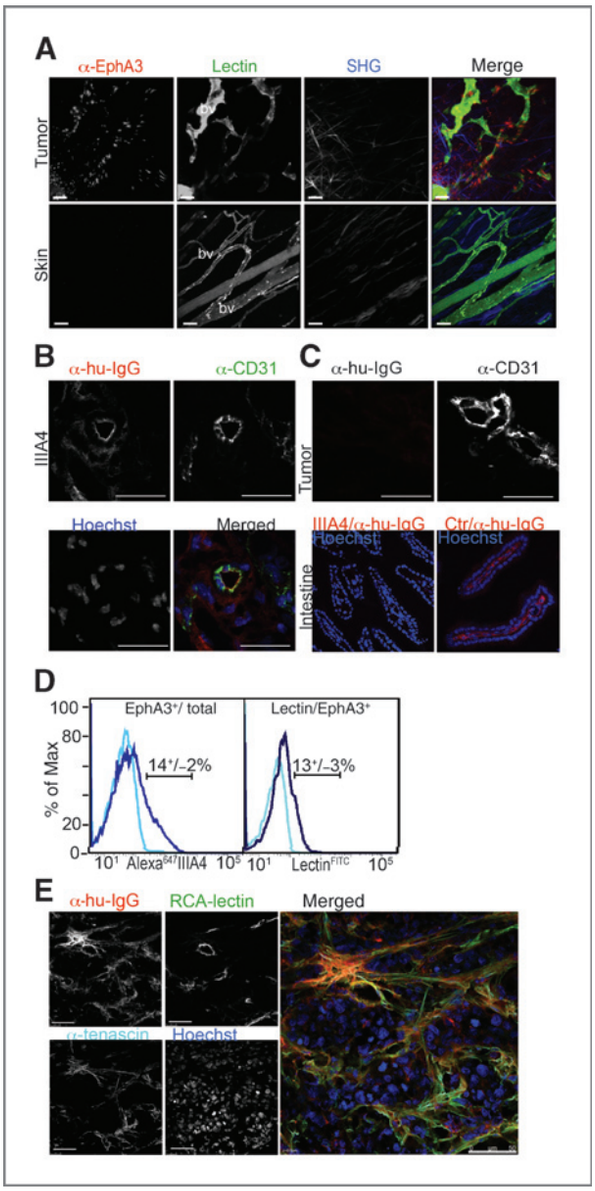

Figure 2. Targeting profile of chIIIA4 antibody in prostate tumor xenografts. A, intravital multiphoton 3D Z-stacks of the rim of DU145 xenografts and adjacent skin, injected 48 hours before imaging with Quantum dot-labeled chIIIA4 antibody (red) and with [FITC]lectin (green), labeling blood vessels. Collagen fibers, detected by second harmonic generation (SHG) signals, are shown in blue. Bottom, adjacent normal mouse from the same mouse; scale bars, 50 μm. B and C, DU145 xenograft tissue sections from mice treated with chIIIA4 (B) or a nonrelevant colon-specific humanized mAb (C) were analyzed with Alexa^{594}-α-human antibodies and FITC-α-CD31 antibodies to assess vascular targeting; scale bars, 25 μm. Bottom, specific binding of the control antibody, but not of IIIA4, to colonic epithelium is illustrated. D, flow cytometry of cell suspensions from DU145 tumor-bearing mice, intravenously injected with [FITC]lectin to label blood-perfused vessels: EphA3$^+$ and [FITC]lectin$^+$ cells as fraction of the total population, lectin$^+$ cells as fraction of the EphA3 cell population were quantitated; mean and SEM are shown ($n \leq 3$ mice/group). E, 22RV1 xenograft tissue sections from mice treated with chIIIA4 (2 × 100 μg) were costained with Alexa^{594}-α-human antibodies, rat α-TNC/Alexa^{568} α-rat antibodies, and RCA-lectin[FITC]; scale bars, 50 μm.

chondrogenic, or adipogenic lineages (Fig. 3B), confirming their multilineage differentiation potential. Supporting our conclusion from these experiments that EphA3$^+$ tumor MSCs are of bone marrow origin, we found elevated levels of EphA3$^+$ cells in bone marrow and in peripheral blood of tumor-bearing mice (Supplementary Fig. S5E).

To further assess the bone marrow origin of the EphA3$^+$ tumor stromal cells, we analyzed tumors from mice that had received bone marrow transplants from transgenic donor mice with ubiquitous GFP expression. Flow cytometry of cell suspensions from early (~0.2 cm^3) tumors revealed a large proportion of EphA3$^+$ cells as part of a tumor-infiltrating GFP$^+$ cell population (Fig. 3C), coexpressing previously assigned cell surface markers, including CD90, CD105, CD106, CD146, CD34, and Sca-1 (Supplementary Fig. S6A). Notably, MACS depletion of EphA3$^+$ cells from the donor bone marrow used for adoptive transfer slowed tumor growth significantly (Fig. 3D). To allow for detection of the bone marrow–derived cells in tumor xenografts, we generated chimeric GFP$^+$/EphA3$^+$ bone marrow for adoptive transfer, by replacing the EphA3$^+$ cells in the donor bone marrow with FACS-isolated transgenic GFP$^+$/EphA3$^+$ cells (Supplementary Fig. S6B and S6C). The tumor growth rate in mice reconstituted with EphA3-depleted bone marrow is reduced compared with mice receiving chimeric donor bone marrow complemented with GFP-EphA3$^+$ cells (Supplementary Fig. S6D). Analysis of tumors from these mice revealed matching immunohistochemical profiles of GFP$^+$ and EphA3$^+$ cells, particularly in the tumor rim (Fig. 3E). Furthermore, confocal microscopy of tumor tissue sections revealed GFP- and EphA3-expressing cells in stromal and perivascular regions of the tumor, which were absent in tumor sections from mice transplanted with non-chimeric bone marrow (Fig. 3F). Together, these findings indicate that EphA3$^+$ bone marrow–derived cells are recruited into the TME and promote tumor growth.

Tumor MSCs respond to EphA3$^+$ activation by cell contraction and apoptosis

Because oncogenic Eph expression frequently coincides with low or absent ephrin expression, while Eph activation is typically tumor suppressive (7, 10, 35), we explored the response of tumor-resident MSCs to EphA3 activation. Analysis of DU145 tumors with EphA3-Fc, a fusion protein that binds EphA3 ligands (36, 37), confirmed lack of EphA3-interacting ephrins in the areas of EphA3 expression and other parts of the tumor (Supplementary Fig. S7A–S7C), suggesting that EphA3 is not ligated in tumor-resident stromal cells.

In vitro activation of Ephs is achieved with preclustered ephrin-Fc fusion proteins (5, 6), but we also demonstrated previously that clustered IIIA4 or synergistic binding of IIIA4 and ephrin-A5 Fc triggers EphA3 activation and cellular responses (23). Thus, while binding of unclustered Alexa^{647} chIIIA4 to cultured EphA3$^+$ MSCs was barely visible, its clustering with α-huFc antibodies significantly increased the cell-bound fluorescence and caused pronounced cell contraction (Fig. 4A–C and Supplementary Fig. S7D). Confocal and Western blot analysis confirmed that chIIIA4 clustering, or its combination with ephrin-A5-Fc, elicits robust EphA3

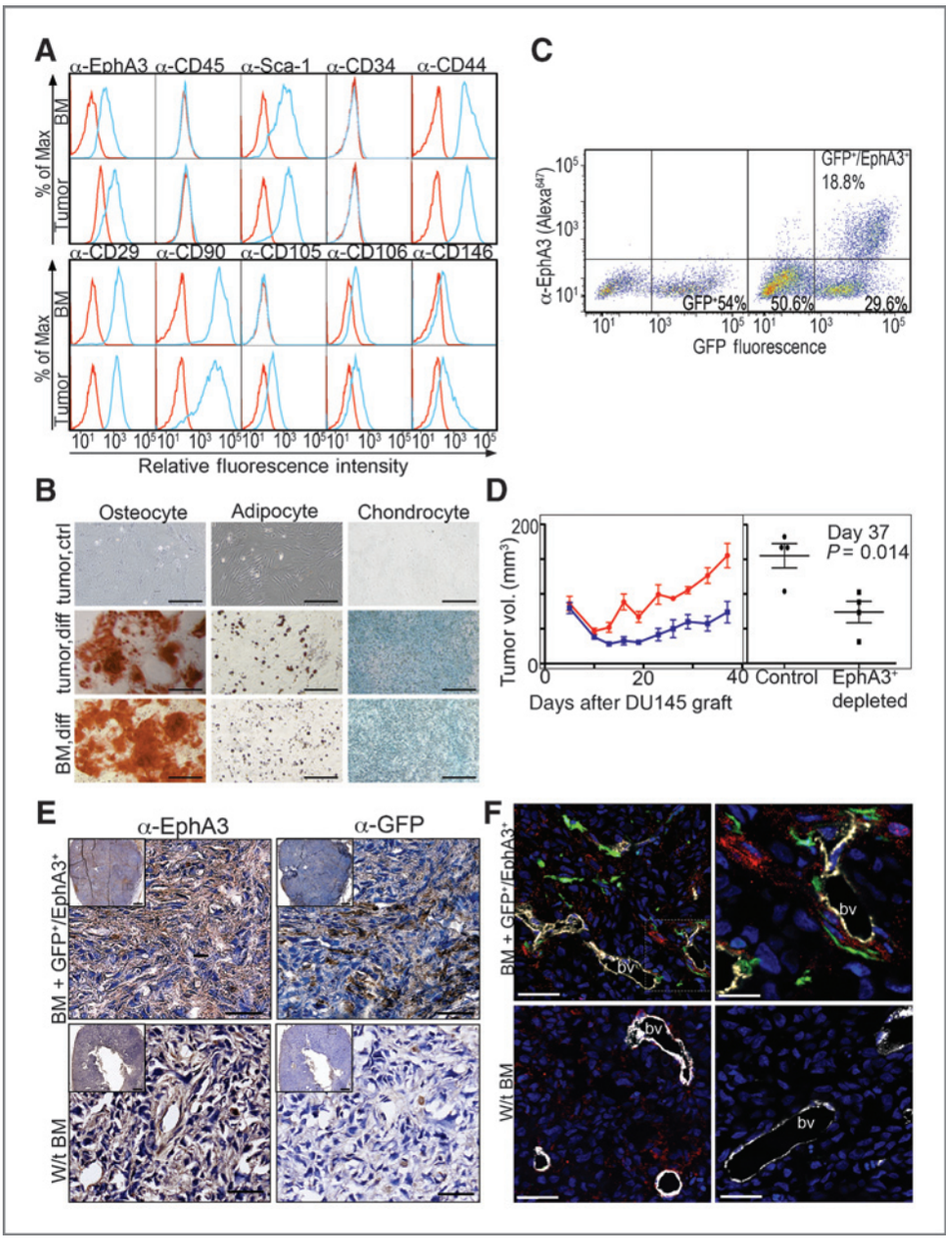

Figure 3. Bone marrow–derived EphA3$^+$ MSCs contribute to the TME. A, comparison by flow cytometry of tumor-derived EphA3$^+$/CD90$^+$/Sca^{Hi} cells, isolated from DU145 tumors (see Supplementary Fig. S5A–S5D), and of EphA3$^+$ BM-MSCs from corresponding tumor-bearing mice. EphA3 coexpression with indicated cell surface markers: chIIIA4-labeled cells (blue) are compared with unstained cells (red). Histograms are representative of three independent experiments. B, multidifferentiation potential of tumor- or bone marrow–derived EphA3$^+$MSCs in control maintenance medium (ctr) or in osteogenic, adipogenic, or chondrogenic differentiation (diff) culture media; staining for osteocyte (alizarin red), adipocyte (oil red O), or chondrocyte (alcian blue) products, respectively. Scale bars, 200 μm. C, single-cell suspensions from DU145 tumors grown in mice after adoptive transfer with EGFP-transgenic bone marrow were assessed for GFP$^+$/EphA3$^+$ cells by flow cytometry; panels illustrate samples unlabeled (left) and Alexa^{647}chIIIA4–labeled cells (right). D, sublethally irradiated mice were reconstituted with bone marrow depleted of EphA3$^+$ cells using Alexa^{647}IIIA4 as capture mAb. Control bone marrow was applied to the MACS system without capture mAb. Tumor growth curves (blue, EphA3-depleted bone marrow; red, control bone marrow) and individual tumor volumes 37 days after grafting are shown; data are representative of three independent experiments. E, tissue sections from Du145 tumor xenografts in mice, transplanted with wild-type (W/t) bone marrow containing FACS-isolated EphA3$^+$ bone marrow cells from GFP$^+$ transgenic mice (see Supplementary Fig. S6B) or W/t bone marrow passed through the FAC sorter without selection. IHC with indicated antibodies (scale bar, 500 μm); insets, boxed areas at 10× resolution (scale bars, 50 μm). F, confocal images of tumor sections from the same group of mice injected with [Rhodamine]lectin to reveal blood-perfused vessels (white pseudo color); sections stained with Alexa^{647}sheep-α-EphA3 (red pseudo color), counterstained with Hoechst (blue, nuclei), GFP$^+$ cells are green (scale bar, 40 μm). Top right, boxed area at increased magnification (scale bar, 20 μm); bottom left, tumor section from W/t nonchimeric bone marrow transplanted mouse; bottom right, control section stained with secondary antibodies (Alexa^{647}sheep-α-EphA3) only.

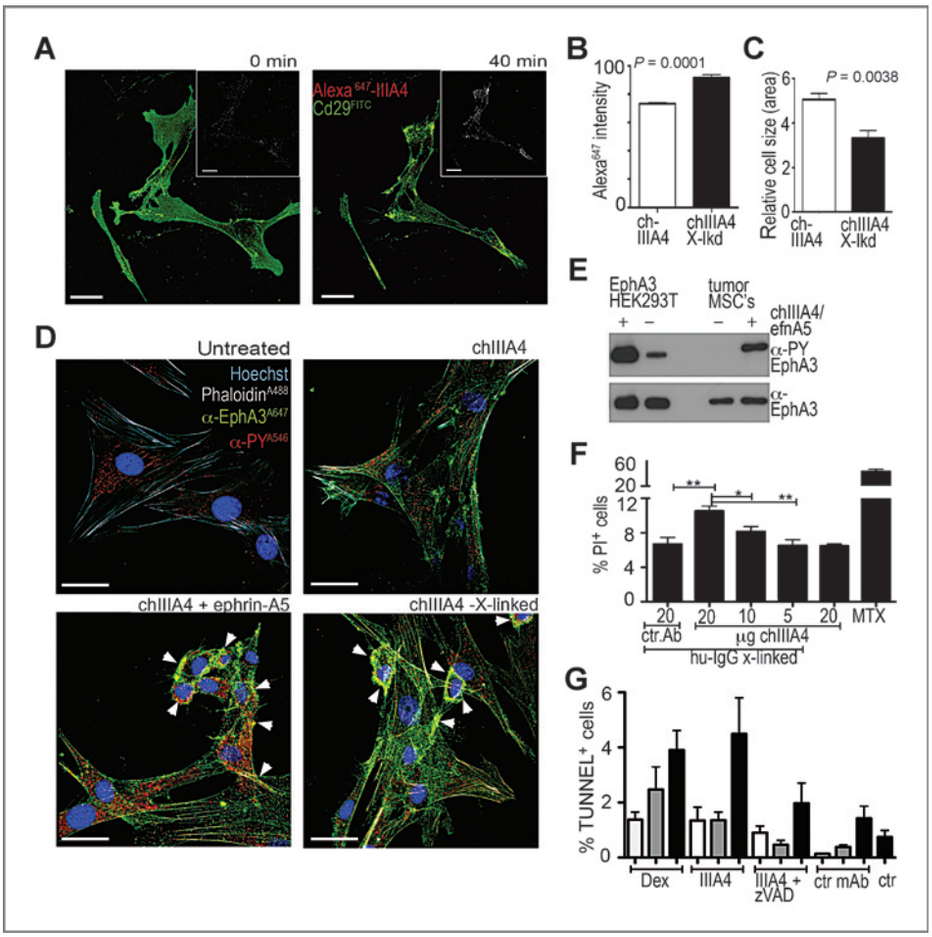

Figure 4. ChIIIA4 triggers cytoskeletal contraction, EphA3 phosphorylation, and apoptosis of tumor-derived EphA3$^+$ MSCs. A, contraction of EphA3$^+$ MSCs after α-FC antibody-mediated clustering of bound Alexa^{647}chIIIA4 (red) over 45 minutes (see Supplementary Fig. S7D); MSCs were developed with α-CD29^{FITC} (insets show Alexa^{647}chIIIA4 only); scale bar, 50 μm; $n = 3$ independent experiments. Estimates of Alexa^{647} fluorescence intensity (B) and relative cell size (C) of $n \geq 20$ cells before and after clustering (X-lkd). D, EphA3 (Alexa^{647}chIIIA4, green) tyrosine phosphorylation (α-PY-Eph/Alexa^{546}α-rabbit, red) and actin cytoskeletal contraction (Alexa^{488}phalloidin, white) following agonist-induced (as indicated) EphA3 clustering; merged confocal images are shown; red/green colocalization appears yellow (arrow heads); nuclei are blue (Hoechst); scale bars, 50 μm. E, α-PY-EphA3 immunoblot analysis of αEphA3 IPs from cells treated with combined chIIIA4/ephrin-A5. Phosphorylation in EphA3/HEK293T cells (23) is shown for comparison. F, EphA3$^+$ MSC viability following treatment with cross-linked (X-linked) or non–cross-linked chIIIA4 was assessed by flow cytometry using propidium iodide uptake. Treatment with methotrexate and a nonrelevant isotype-matched control chimeric antibody (ctr.Ab) were positive and negative controls, respectively; antibody concentrations in μg/mL. Representative results from three independent experiments; *, $P = 0.014$; **, $P = 0.0066$. G, apoptosis in EphA3$^+$ MSCs, treated for 6 hours (□), 8 hours (■), or 12 hours (■) with dexamethasone (10 μmol/L), X-lkd chIIIA4 (20 μg/mL ± zVADfmk), control chimeric antibody (ctr mAb), or low (1%) FCS "starving" media (ctr), was determined with the "Apoptag" TUNEL assay. Apoptotic nuclei in 3 fields of view containing 2–4 × 10^3 cells were quantified (ImageJ) as fraction of Hoechst-positive nuclei. Data are representative of two independent assays; micrographs are shown in Supplementary Fig. S7F.

phosphorylation, cytoskeletal contraction, and cell rounding (Fig. 4D and E). Furthermore, in cocultures of MSCs and DU145 tumor cells, EphA3 activation resulted in a marked dispersion of MSC cell strands (Supplementary Fig. S7E).

We next assessed whether the treatment of EphA3$^+$ tumor MSCs with chIIIA4 would affect their viability. Continuous exposure (48 hours) to preclustered chIIIA4 resulted in a dose-dependent decrease in EphA3$^+$ MSC viability (Fig. 4F). Importantly, this effect was not observed with nonclustered chIIIA4 or a clustered control mAb, where TUNEL staining of chIIIA4-treated MSCs confirmed apoptosis as the underlying mechanism (Fig. 4G and Supplementary Fig. S7F).

ChIIIA4 treatment inhibits tumor growth and disrupts the tumor stromal architecture

To assess the effect of EphA3 targeting *in vivo*, we compared the therapeutic effect of chIIIA4 treatment on established xenografts from EphA3-negative (DU145) or EphA3-positive (22RV1) carcinoma cell lines. Considering that the agonistic activity of chIIIA4 relies on its preclustering with α-Fc antibodies (23), we initially assessed that clustering of cell-bound chIIIA4 by Fc-γ receptor-mediated binding of mouse effector cells (monocytes/macrophages, neutrophils) would cause EphA3 activation. Indeed, chIIIA4 bound to peripheral blood monocytes isolated from BALB/c$^{nu/nu}$ mice in an FcγII/III-

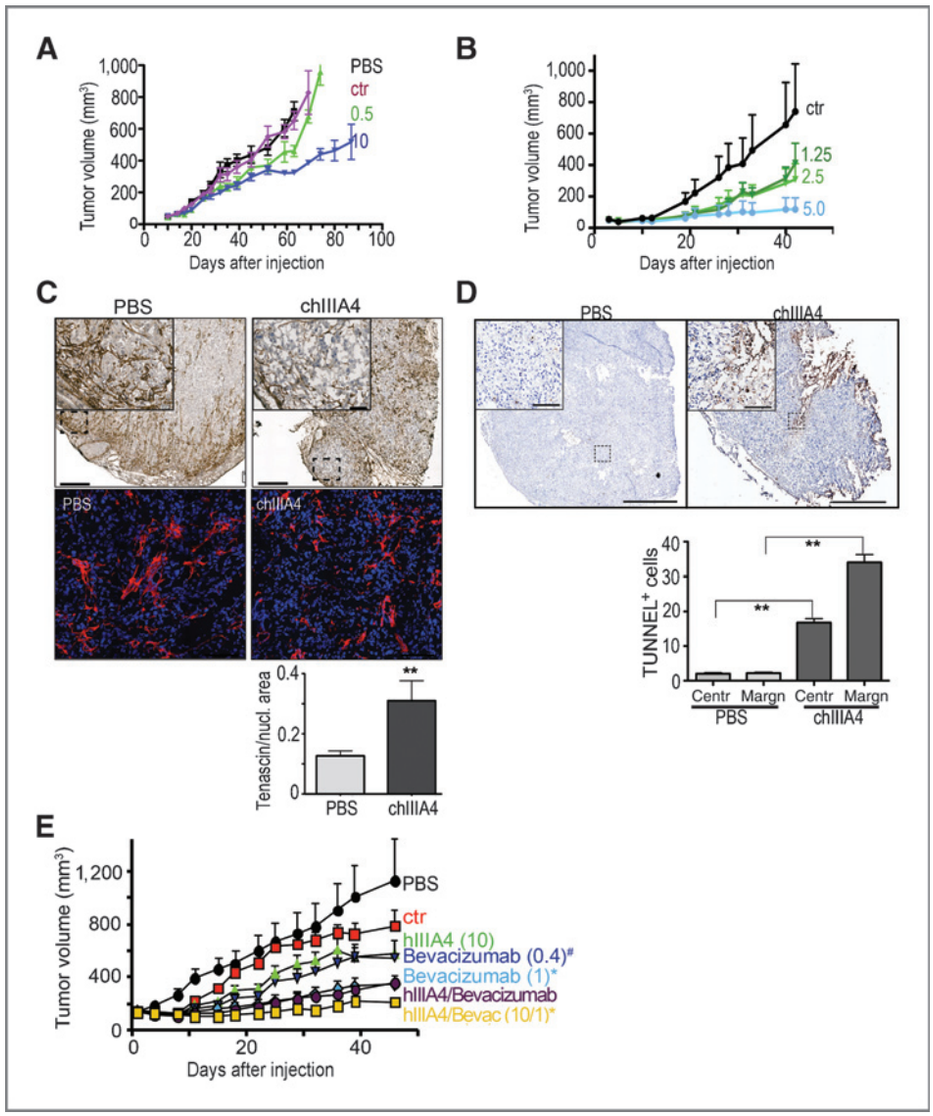

Figure 5. chIIIA4 treatment inhibits tumor growth. Mice bearing Du145 ($n = 10$/group; A) or 22Rv1 tumor xenografts ($n = 6$/group; B) were treated (2× i.p./week) with PBS, control antibody (ctr) or chIIIA4 at indicated concentrations (mg/kg). Tumor volumes: *, $P < 0.05$ between chIIIA4 and PBS groups, days 32 to 63 in A. C, the (DU145) tumor stroma from mice treated with PBS or 10 mg/kg chIIIA4 was assessed by α-Tenascin IHC (top) or IFM (bottom). Top, whole tumor sections (scale bar, 0.5 mm); insets, boxed areas at 10× (scale bar, 50 μm). Bottom, merged fluorescent channels from IFM of sections stained with α-Tenascin/Alexa^{568} α-rat antibodies, counterstained with Hoechst (nuclei); scale bar, 100 μm. Graph, stromal densities were determined (>10 fields of view/tumor, ≥3 mice/group) using ImageJ, mean and SEM; **, $P \geq 0.005$ are shown. D, cell death was assessed using TUNEL IHC. Scale bar, 1 mm; insets, boxed areas at 5× resolution; scale bar, 0.1 mm. TUNEL-positive cells ($n \geq 3$ mice/group, 10 fields of view, each) in tumor margin and center. Mean and SEM; **, $P = 0.0001$ are shown. E, the effects of targeting tumor vasculature with α-EphA3/α-VEGF antibody combinations was assessed in DU145 tumor-bearing mice ($n = 10$/group) treated intraperitoneally with PBS, control IgG1 (ctr, 10 mg/kg), huIIIA4 (10 mg/kg), bevacizumab (Bevac, 0.4 or 1 mg/kg), and indicated combinations. Mean and SEM of tumor volumes; *, $P < 0.05$ between treated and vehicle groups for days 4 to 46; #, $P < 0.05$ from day 8 to 22.

specific manner (Supplementary Fig. S8A), whereas combined treatment of EphA3^{+} MSCs with chIIIA4 and effector cells caused pronounced EphA3 activation and cell contraction (Supplementary Fig. S8B).

Importantly, chIIIA4 treatment of the mice caused a dose-dependent inhibition of both, 22RV1 and DU145 xenograft growth (Fig. 5A and B). IHC and IFM of treated tumors indicated a pronounced disruption of the stromal tumor architecture, where loss of defined stromal strands resulted in dispersed tenascin staining (Fig. 5C). Not surprisingly, chIIIA4 treatment had a dramatic effect on cell viability, and comparative analysis revealed a significant increase in apoptotic cells, particularly in the margin of chIIIA4-treated tumors (Fig. 5D).

In view of its preferential targeting of the vascularized TME, we assessed whether the antitumor effect of IIIA4 could be enhanced by combination treatment with bevacizumab, an approved humanized VEGF-neutralizing and antiangiogenic antibody (38). Indeed, at bevacizumab concentrations, only partially inhibiting DU145 tumor growth, addition of hIIIA4, the humaneered version of chIIIA4 (24), enhanced the antitumor activity and almost completely inhibited DU145 xenograft growth at a ratio of 1:10 mg/kg bevacizumab/hIIIA4 (Fig. 5E).

ChIIIA4 disrupts the architecture and function of tumor microvessels

We next analyzed the effect of chIIIA4 on the tumor microvasculature. IHC and IFM of tumor sections revealed a significantly reduced microvascular density and frequently collapsed vessels (Fig. 6A and Supplementary Fig. S8C and S8D). We therefore used multiphoton microscopy to monitor treatment effects on stromal and microvascular integrity *in vivo*. Imaging of PBS-treated tumors confirmed prominent binding of Qdot^{655}-chIIIA4 to [FITC]lectin-labeled tumor microvessels and to collagen fibers. In contrast, the tumor

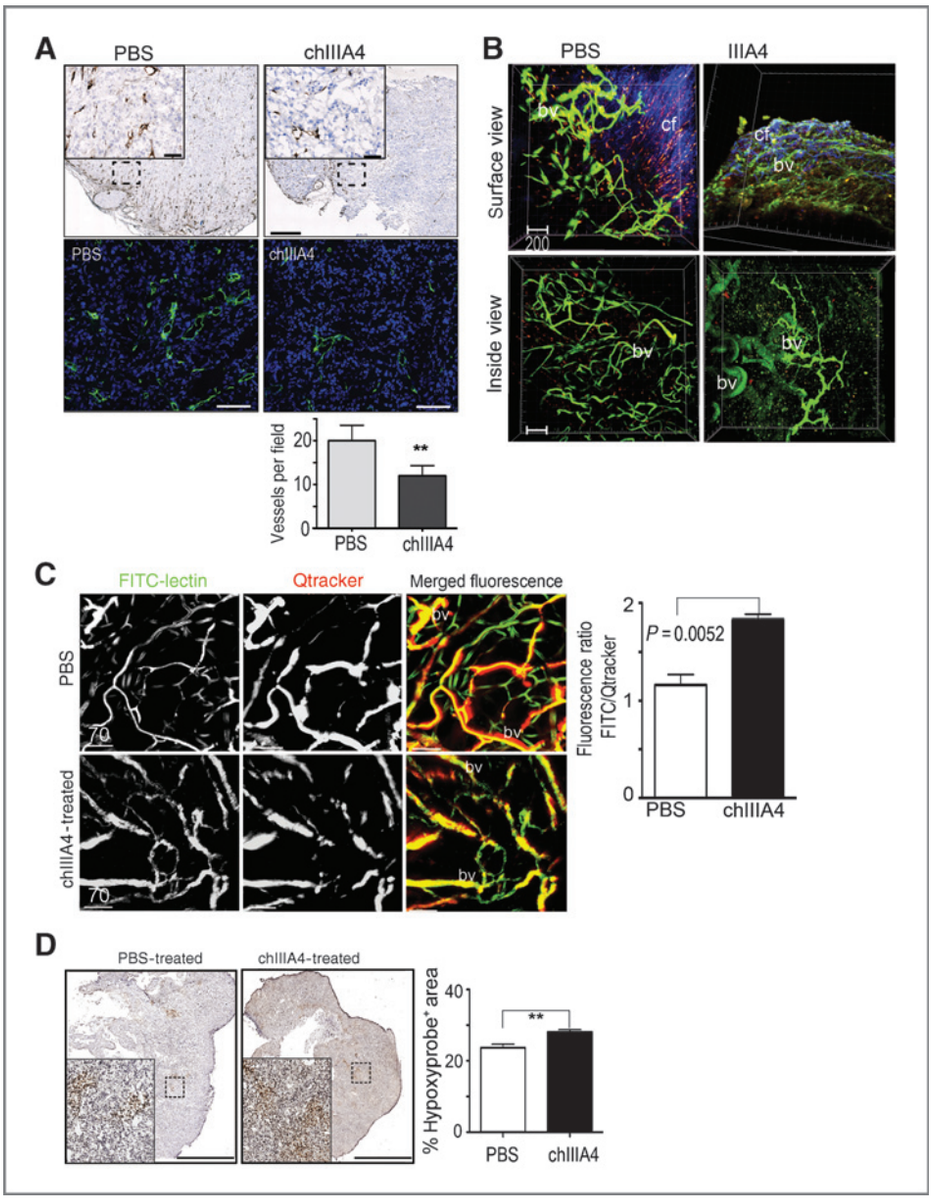

Figure 6. ChIIIA4 disrupts integrity and function of tumor vessels. A, α-CD31 IHC (top) or IFM (bottom) of frozen DU145 tumor sections from mice treated with PBS or 10 mg/kg chIIIA4. Top, whole tumor sections (scale bars, 0.5 mm); insets, boxed areas at 10× (scale bars, 50 μm). Bottom, merged fluorescent channels of α-CD31^{FITC}/Alexa^{488} α-FITC staining (vessels) and Hoechst counterstaining (nuclei); scale bars, 100 μm. Vascular and stromal densities were determined (>10 fields of view/tumor, ≥3 mice/group) using ImageJ; mean and SEM are shown; **, $P \geq 0.005$. B, subcutaneous DU145 tumors, exposed on skin flaps, imaged by intravital multiphoton microscopy. Mice were injected with [Qdot^{655}]chIIIA4 (red) 48 hours before and RCA-lectin[FITC] (green) 5 minutes before analysis; tumor capsule/collagen fibers are revealed by second harmonics generation (blue; ref. 27). C, vessel perfusion in mice injected 30 minutes before imaging with [FITC]lectin (green) and nontargeted QDots^{655} (Qtracker, Invitrogen) labeling the blood (red). FITC/QDot fluorescence ratios were determined from 3D volume-rendered 2-Photon Z-stacks using IMARIS software. D, tumor hypoxia was assessed with α-pimidizole mAb^{FITC}/α-FITC-HRP secondary antibodies and quantitated in tumor sections ($n \geq 3$ mice/group, 10 fields of view, each; **, $P = 0.0002$) using CellSens software.

capsule of chIIIA4-treated tumors was "collapsed," had barely discernible collagen fibers, and severely disrupted tumor microvessels (Fig. 6B), whereas minimal Qdot^{655}chIIIA4 staining suggested that therapeutic chIIIA4 was occupying most of the EphA3-binding sites (Supplementary Fig. S4C).

We examined the vascular disruption suggested from these experiments, by using nonconjugated Qdots^{655} (Qtracker; Invitrogen) to track the blood perfusion in lectin-labeled tumor microvessels after a two-week chIIIA4 treatment. Compared with PBS-treated control mice with a typical contorted tumor microvasculature, the tumor microvessels of treated mice were collapsed, unevenly stained with [FITC]lectin and only partially perfused (Fig. 6C). An approximate doubling in the ratio of [FITC]lectin/Qtracker-fluorescence in treated tumors indicated significantly reduced perfusion of tumor microvessels in chIIIA4-treated mice. In agreement with the extensive damage to the microvessels in the tumor rim suggested from these experiments, we observed a significant increase in hypoxic tumor tissue particularly in the tumor margin, potentially reflecting the reduced oxygenation in regions with compromised tumor vasculature (Fig. 6D).

ChIIIA4 treatment causes a significant reduction in tumor MSCs

We next characterized the *in vivo* response to chIIIA4 in the TME at a cell/biochemical level. In agreement with the observation that clustered chIIIA4 activates EphA3^{+} tumor MSCs *in vitro*, IP/Western blot analysis of tumor lysates revealed that chIIIA4 treatment leads to transient EphA3 phosphorylation

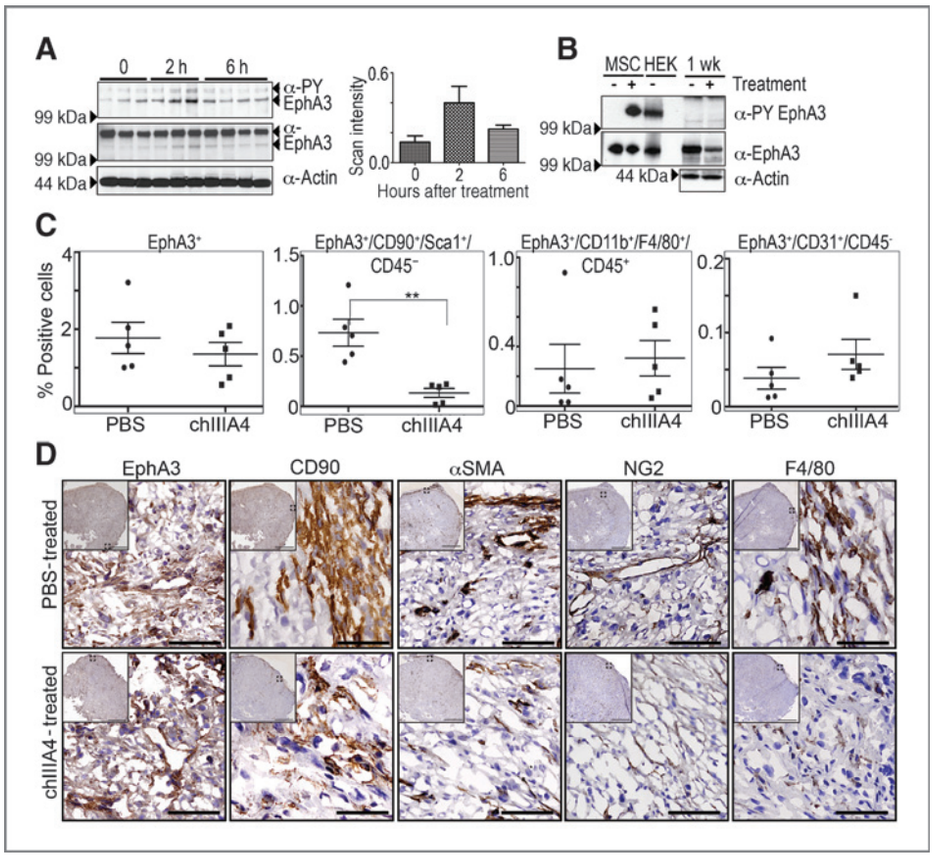

Figure 7. Effects of chIIIA4 on EphA3$^+$ MSCs and the TME. A, α-EphA3 and α-phospho (PY) EphA3 immunoblot analysis of α-EphA3 IPs from tumors, resected at indicated times following a single 10 mg/kg chIIIA4 injection. Arrows indicate positions of (full-length and truncated) EphA3 and of phospho-EphA3. B, immunoblot analysis of tumors after 1 week (wk) treatment; actin immunoblots of lysates serve as loading control. IPs from MSCs and EphA3-HEK293T cells (HEK), treated as indicated, were analyzed in parallel. C, DU145 tumor cell suspensions from mice ($n = 5$/group) treated with chIIIA4 or PBS were analyzed by flow cytometry. Data are representative of two independent experiments; **, $P = 0.003$. D, IHC with antibodies against EphA3 (sheep-α-EphA3), stromal (α-CD90), perivascular (α-smooth muscle actin, α-NG2), and myeloid (α-F4/80) markers; insets show overviews and the positions of magnified areas are boxed (scale bars, 1 mm, 50 μm).

within tumors 2 hours after injection (Fig. 7A). Interestingly, after 1 week of chIIIA4 treatment, the overall EphA3 protein levels in DU145 tumors were notably reduced and did not reveal detectable EphA3 phosphorylation (Fig. 7B and Supplementary Fig. S8E). We therefore assessed the cell type within the TME that was mainly targeted by chIIIA4. After 2-week treatment, we noted a significant reduction in the fraction of EphA3$^+$Sca-1$^+$CD90$^+$CD45$^-$ cells (Fig. 7C), consistent with IIIA4 affecting the viability of EphA3$^+$ MSCs *in vitro* (Fig. 4F and G). Overall, this resulted in a slight decrease in EphA3$^+$ cells. In agreement with the effect of chIIIA4 on EphA3$^+$ MSC viability *in vitro* and *in vivo*, and on the overall integrity of the tumor stroma, IHC of xenograft sections revealed notably disrupted patterns of stromal (CD90), perivascular (NG2, smooth muscle actin), and myeloid/macrophage marker proteins in the tumor rim of chIIIA4-treated tumors (Fig. 7D).

Discussion

Eph receptors are implicated in growth and progression of a large range of cancers (4, 5). We now demonstrate for the first time the prominent expression and function of EphA3 in the TME of tumor xenografts and human sections, but virtually undetectable expression in normal adult tissues and organs. We show that bone marrow–derived EphA3$^+$ stromal cells are recruited into the TME where they contribute to nascent vascular and stromal tissues. Treatment with chIIIA4, a highly specific mAb and selective EphA3 agonist (29–31), elicits EphA3 kinase activation, cell contraction, and apoptosis of tumor-resident MSCs, and inhibits tumor growth by disruption of the architecture and function of the vascularized TME.

EphA3 activation inhibits tumor growth

Our demonstration that activation of EphA3 with chIIIA4 effectively inhibits tumor growth seems at odds with a range of reports where its overexpression in various cancers has been correlated with disease progression and poor prognosis (9, 15–17). However, Ephs are known for their context-dependent, dichotomous functions (4, 5): typically, kinase-dormant Ephs promote cell–cell adhesion, invasion, and tumor (stem cell) maintenance and are regarded oncogenic (4–6, 39), whereas Eph kinase activation is tumor suppressive by causing cell–cell segregation and reduced viability (7, 32, 40). Thus, overexpression of kinase-dormant EphA3 in glioblastoma acts to maintain tumor cells in a dedifferentiated, tumorigenic state, whereas activation of its kinase inhibits glioma cell proliferation (9). In agreement, our studies suggest that EphA3, overexpressed in tumor MSCs and other stromal cells with a dormant kinase, functions in the development of the TME and that its pharmacologic activation results in TME disruption and suppressed tumor growth. Necessarily, this kinase-dormant EphA3 function implies the absence of interacting ephrins, which is in agreement with previous reports,

suggesting exclusive oncogenic overexpression of either Ephs or ephrins (7, 10). We found no evidence for EphA3-binding ephrins in the analyzed tumors.

The IIIA4 mAb targets tumor-derived MSCs and disrupts tumor stromal and vascular integrity

Considering the reported expression of EphA3 in a range of tumor cells (9, 15–17, 41), the most prominent tumor stromal EphA3 expression described here is noteworthy. Thus, while our analysis of human tumor tissues confirmed the previously reported tumor cell expression in glioblastoma and colon cancer (9, 41), our survey revealed significantly more pronounced and frequent EphA3 expression in the tumor stroma of all analyzed cancers, a pattern that is consistent with its involvement in the formation of the TME. Consistent with this previously unrecognized role, an interim report from ongoing clinical studies of humaneered IIIA4 (KB004) in leukemias shows responses in one of the patients that also suggest targeting of the stromal/fibrotic TME (24).

Our experiments demonstrate EphA3 expression on bone marrow–derived MSCs and myeloid cell types. Considering the multilineage potential and phenotypic plasticity of MSCs, allowing their differentiation into mesenchymal and vascular lineages, and their direct contribution to adult neovascularization (42, 43), it is tempting to speculate that the EphA3$^+$ MSCs in our studies may be progenitors for several or all of the tumor-infiltrating stromal cell types. EphA3 was previously identified among the hypoxia-regulated genes of human bone marrow–derived MSCs (44), and the notion of EphA3$^+$ mesenchymal progenitor cells, differentiating within the TME into different EphA3$^+$ stromal cell populations, concurs with its embryonic expression on mesodermal (12), vascular, and mesenchymal tissues (11, 45) and its essential role in EndMT during heart valve development (14). In support of this premise, we found that bone marrow–derived and tumor-derived EphA3$^+$ MSCs from tumor-bearing mice have the same phenotypic and pluripotent functional characteristics, and confirmed by adoptive bone marrow transfer the bone marrow origin of tumor-resident EphA3$^+$ MSCs.

Together with the notable lack of EphA3 expression in nontumor adult tissues, our data suggest EphA3 as a novel marker, both of MSCs and of tumor stromal tissue. Considering its developmental role in EndMT (14) and the recently reported involvement of EphB2 signaling in MSC adhesion, migration, and differentiation (46), it will be of interest to understand the potential involvement of EphA3 in MSC mobilization, recruitment into tumors, and multilineage differentiation capacity.

In conclusion, the notable stromal expression of EphA3 in the vast majority of analyzed human tumor samples and lack of expression in normal adult tissues, together with the targeting specificity and antitumor properties of the chIIIA4 mAb, define EphA3 as attractive target for antibody-based anticancer therapies. The promising clinical responses of the humaneered therapeutic IIIA4 antibody, KB004, in ongoing phase I/II trials (NCT01211691; ref. 24) therefore suggest immediate therapeutic opportunities for the treatment of solid tumors.

Disclosure of Potential Conflicts of Interest

M. Baer has ownership interest (including patents) in KaloBios Pharmaceuticals. V. Palath has ownership interest (including patents) in KaloBios Pharmaceuticals. C. Bebbington has ownership interest (including patents) in KaloBios Pharmaceuticals. G. Yarranton received commercial research support from and has ownership interest (including patents) in KaloBios Pharmaceuticals. A.M. Scott received a commercial research grant from Kalobios Pharmaceuticals. No potential conflicts of interest were disclosed by the other authors.

Authors' Contributions

Conception and design: M.E. Vail, A. Tan, D. Abebe, C. Bebbington, G. Yarranton, A.M. Scott, M. Lackmann

Development of methodology: M.E. Vail, C. Murone, A. Tan, L. Hii, D. Abebe, F.-T. Lee, V. Palath, A.M. Scott, M. Lackmann

Acquisition of data (provided animals, acquired and managed patients, provided facilities, etc.): M.E. Vail, A. Tan, L. Hii, D. Abebe, P.W. Janes, F.-T. Lee, M. Baer, G. Cartwright, A.M. Scott, M. Lackmann

Analysis and interpretation of data (e.g., statistical analysis, biostatistics, computational analysis): M.E. Vail, C. Murone, A. Tan, L. Hii, D. Abebe, P.W. Janes, F.-T. Lee, M. Baer, G. Yarranton, D. Abramson, G. Cartwright, A.M. Scott, M. Lackmann

Writing, review, and/or revision of the manuscript: M.E. Vail, A. Tan, V. Palath, C. Bebbington, A.M. Scott, M. Lackmann

Administrative, technical, or material support (i.e., reporting or organizing data, constructing databases): M.E. Vail, C. Murone, A. Tan, C. Llerena, S. Garic, A.M. Scott, M. Lackmann

Study supervision: M.E. Vail, F.-T. Lee, V. Palath, C. Bebbington, A.M. Scott, M. Lackmann

Acknowledgments

The authors thank Dr. Peter Crowley, senior Anatomical Pathologist at Austin Health, for expert interpretation of IHC and IFM tissue sections. The biospecimen and associated clinical data used in this project were provided by the Victorian Cancer Biobank with appropriate ethics approval. The Victorian Cancer Biobank is supported by the Victorian Government. The authors also thank I. Harper (Monash Micro Imaging) and A. Fryga (Monash Flowcore) for technical support, Dr. M. Hickey for intravital microscopy advice, Chanley Chheang for cell viability and IHC assays, A. Perani, B. Gloria, R. Murphy for antibody production, and A. Rigopoulos and D. Cao for help with animal experiments. Studies using bevacizumab were conducted at BioQuant Inc, San Diego, California. This manuscript is dedicated to the life and memory of Martin Lackmann, November 3, 1956 to May 22, 2014.

Grant Support

This work was supported by grants from the NH&MRC (nos. 487922 and 1049942), Cancer Australia and Prostrate Cancer Foundation Australia (no. 491195; to M. Lackmann and A.M. Scott), The Human Frontiers Science Program (to M. Lackmann), funds from the Operational Infrastructure Support Program provided by the Victorian Government, Australia (to A.M. Scott), and KaloBios Pharmaceuticals (to M. Lackmann and A.M. Scott). M. Lackmann is an NH&MRC Senior Research Fellow.

The costs of publication of this article were defrayed in part by the payment of page charges. This article must therefore be hereby marked *advertisement* in accordance with 18 U.S.C. Section 1734 solely to indicate this fact.

Received January 24, 2014; revised April 7, 2014; accepted May 12, 2014; published online August 14, 2014.

References

1. Hanahan D, Coussens LM. Accessories to the crime: functions of cells recruited to the tumor microenvironment. Cancer Cell 2012;21:309–22.
2. McAllister SS, Weinberg RA. Tumor-host interactions: a far-reaching relationship. J Clin Oncol 2010;28:4022–8.
3. Gao D, Mittal V. The role of bone-marrow-derived cells in tumor growth, metastasis initiation and progression. Trends Mol Med 2009;15:333–43.
4. Boyd AW, Bartlett PF, Lackmann M. Therapeutic targeting of EPH receptors and their ligands. Nat Rev Drug Discov 2014;13:39–62.

5. Pasquale EB. Eph receptors and ephrins in cancer: bidirectional signalling and beyond. Nat Rev Cancer 2010;10:165–80.
6. Nievergall E, Lackmann M, Janes PW. Eph-dependent cell-cell adhesion and segregation in development and cancer. Cell Mol Life Sci 2012;69:1813–43.
7. Noren NK, Foos G, Hauser CA, Pasquale EB. The EphB4 receptor suppresses breast cancer cell tumorigenicity through an Abl-Crk pathway. Nat Cell Biol 2006;8:815–25.
8. Genander M, Halford MM, Xu NJ, Eriksson M, Yu Z, Qiu Z, et al. Dissociation of EphB2 signaling pathways mediating progenitor cell proliferation and tumor suppression. Cell 2009;139:679–92.
9. Day BW, Stringer BW, Al-Ejeh F, Ting MJ, Wilson J, Ensbey KS, et al. EphA3 maintains tumorigenicity and is a therapeutic target in glioblastoma multiforme. Cancer Cell 2013;23:238–48.
10. Macrae M, Neve RM, Rodriguez-Viciana P, Haqq C, Yeh J, Chen C, et al. A conditional feedback loop regulates Ras activity through EphA2. Cancer Cell 2005;8:111–8.
11. Kilpatrick TJ, Brown A, Lai C, Gassmann M, Goulding M, Lemke G. Expression of the Tyro4/Mek4/Cek4 gene specifically marks a subset of embryonic motor neurons and their muscle targets. Mol Cell Neurosci 1996;7:62–74.
12. Oates AC, Lackmann M, Power MA, Brennan C, Down LM, Do C, et al. An early developmental role for eph-ephrin interaction during vertebrate gastrulation. Mech Dev 1999;83:77–94.
13. Gallarda BW, Bonanomi D, Muller D, Brown A, Alaynick WA, Andrews SE, et al. Segregation of axial motor and sensory pathways via heterotypic trans-axonal signaling. Science 2008;320:233–6.
14. Stephen LJ, Fawkes AL, Verhoeve A, Lemke G, Brown A. A critical role for the EphA3 receptor tyrosine kinase in heart development. Dev Biol 2007;302:66–79.
15. Chiari R, Hames G, Stroobant V, Texier C, Maillere B, Boon T, et al. Identification of a tumor-specific shared antigen derived from an Eph receptor and presented to CD4 T cells on HLA class II molecules. Cancer Res 2000;60:4855–63.
16. Xi HQ, Wu XS, Wei B, Chen L. Aberrant expression of EphA3 in gastric carcinoma: correlation with tumor angiogenesis and survival. J Gastroenterol 2012;47:785–94.
17. Keane N, Freeman C, Swords R, Giles FJ. EPHA3 as a novel therapeutic target in the hematological malignancies. Expert Rev Hematol 2012;5:325–40.
18. Ashton JM, Balys M, Neering SJ, Hassane DC, Cowley G, Root DE, et al. Gene sets identified with oncogene cooperativity analysis regulate *in vivo* growth and survival of leukemia stem cells. Cell Stem Cell 2012;11:359–72.
19. Lisabeth EM, Fernandez C, Pasquale EB. Cancer somatic mutations disrupt functions of the EphA3 receptor tyrosine kinase through multiple mechanisms. Biochemistry 2012;51:1464–75.
20. Sjoblom T, Jones S, Wood LD, Parsons DW, Lin J, Barber TD, et al. The consensus coding sequences of human breast and colorectal cancers. Science 2006;314:268–74.
21. Ding L, Getz G, Wheeler DA, Mardis ER, McLellan MD, Cibulskis K, et al. Somatic mutations affect key pathways in lung adenocarcinoma. Nature 2008;455:1069–75.
22. Balakrishnan A, Bleeker FE, Lamba S, Rodolfo M, Daniotti M, Scarpa A, et al. Novel somatic and germline mutations in cancer candidate genes in glioblastoma, melanoma, and pancreatic carcinoma. Cancer Res 2007;67:3545–50.
23. Vearing C, Lee FT, Wimmer-Kleikamp S, Spirkoska V, To C, Stylianou C, et al. Concurrent binding of anti-EphA3 antibody and ephrin-A5 amplifies EphA3 signaling and downstream responses: potential as EphA3-specific tumor-targeting reagents. Cancer Res 2005;65:6745–54.
24. Lancet J, Wei AH, Durrant ST, Hertzberg MS, Swords RT, Lewis ID, et al. A phase I study of KB004, a novel non-fucosylated humaneered® antibody, targeted against the receptor tyrosine kinase EphA3, in advanced hematologic malignancies [abstract]. In: Proceedings of the 55th ASH Annual Meeting and Exposition; 2013 Dec 7–10; New Orleans, LA. Washington, DC: ASH; 2013. Abstract nr 3838.
25. Palmieri M, Nowell CJ, Condron M, Gardiner J, Holmes AB, Desai J, et al. Analysis of cellular phosphatidylinositol (3,4,5)-trisphosphate levels and distribution using confocal fluorescent microscopy. Anal Biochem 2010;406:41–50.
26. di Tomaso E, Capen D, Haskell A, Hart J, Logie JJ, Jain RK, et al. Mosaic tumor vessels: cellular basis and ultrastructure of focal regions lacking endothelial cell markers. Cancer Res 2005;65:5740–9.
27. Zipfel WR, Williams RM, Webb WW. Nonlinear magic: multiphoton microscopy in the biosciences. Nat Biotechnol 2003;21:1369–77.
28. Russel ABM, Abramson D, Bethwaite B, Minh Ngoc D, Enticott C, Firth S, et al. An abstract virtual instrument system for high throughput automatic microscopy.ICCS 2010;1:545–54.
29. Boyd AW, Ward LD, Wicks IP, Simpson RJ, Salvaris E, Wilks A, et al. Isolation and characterization of a novel receptor-type protein tyrosine kinase (hek) from a human pre-B cell line. J Biol Chem 1992;267:3262–7.
30. Smith FM, Vearing C, Lackmann M, Treutlein H, Himanen J, Chen K, et al. Dissecting the EphA3/Ephrin-A5 interactions using a novel functional mutagenesis screen. J Biol Chem 2004;279:9522–31.
31. Vearing CJ, Lackmann M. "Eph receptor signalling; dimerisation just isn't enough". Growth Factors 2005;23:67–76.
32. Lawrenson ID, Wimmer-Kleikamp SH, Lock P, Schoenwaelder SM, Down M, Boyd AW, et al. Ephrin-A5 induces rounding, blebbing and de-adhesion of EphA3- expressing 293T and melanoma cells by CrkII and Rho-mediated signalling. J Cell Sci 2002;115:1059–72.
33. Morikawa S, Mabuchi Y, Kubota Y, Nagai Y, Niibe K, Hiratsu E, et al. Prospective identification, isolation, and systemic transplantation of multipotent mesenchymal stem cells in murine bone marrow. J Exp Med 2009;206:2483–96.
34. Zhu H, Guo ZK, Jiang XX, Li H, Wang XY, Yao HY, et al. A protocol for isolation and culture of mesenchymal stem cells from mouse compact bone. Nat Protoc 2010;5:550–60.
35. Batlle E, Bacani J, Begthel H, Jonkheer S, Gregorieff A, van de Born M, et al. EphB receptor activity suppresses colorectal cancer progression. Nature 2005;435:1126–30.
36. Gale NW, Holland SJ, Valenzuela DM, Flenniken A, Pan L, Ryan TE, et al. Eph receptors and ligands comprise two major specificity subclasses and are reciprocally compartmentalized during embryogenesis. Neuron 1996;17:9–19.
37. Genander M, Holmberg J, Frisen J. Ephrins negatively regulate cell proliferation in the epidermis and hair follicle. Stem Cells 2010;28:1196–205.
38. Ellis LM, Hicklin DJ. VEGF-targeted therapy: mechanisms of anti-tumour activity. Nat Rev Cancer 2008;8:579–91.
39. Batlle E, Wilkinson DG. Molecular mechanisms of cell segregation and boundary formation in development and tumorigenesis. Cold Spring Harb Perspect Biol 2012;4:a008227.
40. Cortina C, Palomo-Ponce S, Iglesias M, Fernandez-Masip JL, Vivancos A, Whissell G, et al. EphB-ephrin-B interactions suppress colorectal cancer progression by compartmentalizing tumor cells. Nat Genet 2007;39:1376–83.
41. Xi HQ, Zhao P. Clinicopathological significance and prognostic value of EphA3 and CD133 expression in colorectal carcinoma. J Clin Pathol 2011;64:498–503.
42. Bianco P, Robey PG, Simmons PJ. Mesenchymal stem cells: revisiting history, concepts, and assays. Cell Stem Cell 2008;2:313–9.
43. Lin CS, Lue TF. Defining vascular stem cells. Stem Cells Dev 2013;22:1018–26.
44. Martin-Rendon E, Hale SJ, Ryan D, Baban D, Forde SP, Roubelakis M, et al. Transcriptional profiling of human cord blood CD133+ and cultured bone marrow mesenchymal stem cells in response to hypoxia. Stem Cells 2007;25:1003–12.
45. Kawakami Y, Uchiyama Y, Rodriguez Esteban C, Inenaga T, Koyano-Nakagawa N, Kawakami H, et al. Sall genes regulate region-specific morphogenesis in the mouse limb by modulating Hox activities. Development 2009;136:585–94.
46. Arthur A, Zannettino A, Panagopoulos R, Koblar SA, Sims NA, Stylianou C, et al. EphB/ephrin-B interactions mediate human MSC attachment, migration and osteochondral differentiation. Bone 2011;48:533–42.